Invited paper

Radio wave propagation and single-cell coverage prediction of broadband radio access systems including passive reflectors

Georg Bauer, Jens Freese, and Rolf Jakoby

Abstract — This paper presents the scheme of a software planing tool for single microcells of broadband radio access systems operating at millimeter waves, providing local multipoint distribution services (LMDS), particularly in urban or suburban areas. The aim of this planing tool is to provide operators with information, which supports the assessment of the profitability by calculating link budgets and the area coverage and by roughly estimating the maximum number of potential customers, i.e. the total number of households in a certain area, as well as the number of customers (households) which will actually be covered from a site. A household is here considered as a single apartment or flat, thus a building usually consists of several households. This novel household-estimation model is able to estimate the number of households based only on the 3D-data of buildings, without using residential data. Besides the optimization of line-of-sight (LOS) coverage, also the possibility is considered to enhance the coverage into shadowed areas by using optimized reflectors as passive repeaters up to distances of 1 km from the base station, depending on the system margin and the rain climate zone. All calculations are based on 3D-databases of both, buildings and vegetation.

Keywords — millimeter wave propagation, LMDS, coverage prediction, passive reflectors.

1. Introduction

Broadband radio access systems operating at millimeter waves, used for local multipoint distribution services, are local cellular point-to-multipoint radio systems, delivering multimedia services and/or broadcast services from a central transmitter or base station to individual houses or blocks of apartments or houses for residential and business customers within its cell size, offering rapid infrastructure deployment and the ability to provide local content. It can be significantly cheaper to install than a cable system since only homes requesting LMDS are provided with receivers (extension on demand). Hence, these LMDS systems can be applied as a supplement of the broadband cable TV network (CATV), as a substitution of the CATV or direct broadcast via satellite (DBS) or as a cable pull through during the building up or extension of parts of the cable networks. For these reasons and because of its flexible installation, LMDS systems have recently gained popularity worldwide, in particular in the USA, Canada and in Eastern Europe.

Figure 1 exhibits an example of a bi-directional cellular LMDS system primarily for broadcast services to residential customers. The different sources, e.g. from satellite, terrestrial VHF/UHF or local contents are collected in a Head End, and then provided to the LMDS base stations via a backbone network, which might consists of radio links in the millimeter wave region, optical fiber or other cable networks. Beyond one-way broadcasting distribution, this wireless technology has the potential 1) for providing expanded TV services like pay per view, near or video on demand as well as, 2) to become a low-cost integrated medium for providing voice and data services, as well, having the potential to integrate the CATV and ISDN networks. This allows fully interactive services such as video conferences and high speed access to Internet. This wireless technology can be a quick, simple and cost-effective solution.

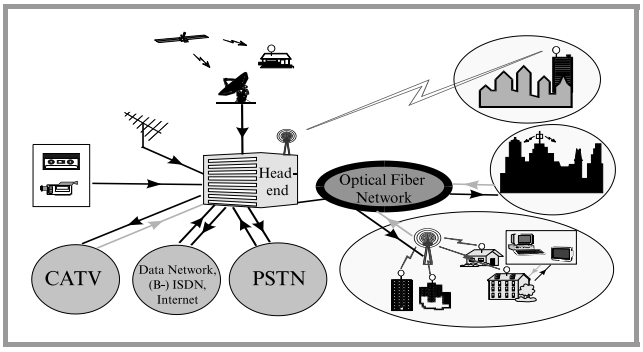

Fig. 1. Example of a bi-directional cellular LMDS system.

Local multipoint distribution services systems at millimeter waves have a large bandwidth of up to 2 GHz but a very limited coverage to a few kilometers only [see Section 3]. This is mainly because they require clear line of sight for reliable point-to-multipoint links between the base station and the subscriber antennas as well as because millimeter waves for LMDS in between 26 GHz and 43 GHz suffer on large propagation losses, particularly free-space propagation losses and attenuation caused by rain as well as large diffraction and reflection losses on buildings.

Hence, in literature, very often only the number of covered buildings within a cell is used to estimate the penetra-

tion rate of a LMDS microcell. It is usually calculated by checking only the roof tops of the buildings for coverage. In general, however, the number of covered buildings does not agree with the number of customers, since there are often several households (customers) in one building, which might be served only via one customer station located on the roof top. However, similar to satellite broadcasting, many customers, in particular residential subscribers, might wish to have direct access to a broadband multimedia wireless network. As a consequence, the percentage of customers that can be covered by one LMDS base station is much lower than the number of covered roof tops. While a roof top coverage (buildings) of up to 70% can usually be achieved in a area range of 1 km around the base station Biddiscombe [3], only $25 \div 35\%$ of the customers (households) can be supplied with a direct access. Even near the base station there are a large number of uncovered households. Therefore, a simple household-estimation model is presented to get more realistic results, and in addition, the use of a shaped metallic reflector is introduced in order to enhance the area coverage into shadowed areas. Both, the household-estimation model and some approximated results of the reflector analysis with physical optics (PO) Diaz [4] have been implemented into a software tool for single-cell LMDS coverage prediction.

2. Example of an unidirectional LMDS system for broadcast services

There are many standardization boards and hence different standards for LMDS worldwide. As a standardization example in Europe, the $40.5 \div 42.5$ GHz band has been harmonized within the CEPT for a multipoint video distribution system (MVDS) or unidirectional LMDS system. The standards for digital 42 GHz MVDS [3] are based on performance specifications from working groups in the UK [7] and the DVB-Adhoc group [2, 8]. Hereafter, the system performs the adaptation of the base band TV signals from the output of the MPEG-2 transport multiplexer to the MVDS channel characteristics. Then, it uses randomization for energy dispersal and a concatenated error protection strategy based on a shortened Reed-Solomon (RS) code with a code rate $r_1 = 188/204 = 0.922$, convolution interleaving and convolution code, in order to provide a quasi error free quality target at the input of the MPEG-2 demultiplexer. The convolution code r_2 is flexible, allowing the optimization of the system performance for a given MVDS transmitter bandwidth, e.g. for 33 MHz, for which the useful bit rate $R_u = r_1 \times r_2 \times R_s$ in Mbit/s is shown in Table 1. To achieve a very high power efficiency without excessively penalizing the spectrum efficiency, MVDS uses base band shaping by applying a square-root raised cosine filter with a roll-off factor of 0.35 ($B_{RF,3\,\mathrm{dB}}/R_S = 1.27$) and QPSK modulation with a symbol rate R_s of 26 Mbaud for 33 MHz. Table 1 exhibits the corresponding required signal-to-noise power ratio at the receiver input as a function of the convolution code r_2 [3].

Table 1
Useful bite rate R_u, energy per bit to noise power, E_b/N_0, and the required signal-to-noise power ratio $S/N_{req} = 2 \cdot r_1 \cdot r_2 \cdot E_b/N_0$ at the receiver input as a function of r_2 for QPSK and a 3-dB-bandwidth of 33 MHz

Parameter	$r_2 = 1/2$	$r_2 = 2/3$	$r_2 = 3/4$	$r_2 = 5/6$	$r_2 = 7/8$
R_u [Mbit/s]	24.0	31.9	35.9	39.9	41.9
E_b/N_0 [dB]	4.5	5.0	5.5	6.0	6.4
S/N_{req} [dB]	4.1	5.9	6.9	7.9	8.5

The allocated 2-GHz-frequency spectrum for digital MVDS is divided 1) into a downstream, including 96 RF-channels with a bandwidth of 33 MHz and a channel spacing of 39 MHz, and 2) into an upstream for return paths, having a bandwidth of 50 MHz at both ends of the 2 GHz band, respectively (Fig. 2). To double the capacity in cellular networks, use is made of vertical and horizontal polarization. Hence, the available spectrum might be separated into four groups of 24 RF-channels for cellular MVDS networks. The frequency error of each carrier shall not exceed ± 0.5 MHz at 40 GHz and the carrier output power shall not exceed 0.5 W (UK) or 1 W (GER) per channel. The power of spurious emission is given in [7]. Many aspects and issues of a one-way MVDS were already been discussed in the DIMMP-Project [2] and some proposals for the upstream issues are made by DAVIC [1] and DVB [4].

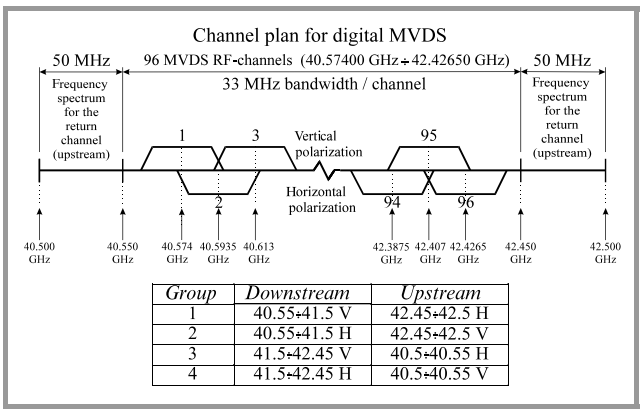

Group	*Downstream*	*Upstream*
1	40.55÷41.5 V	42.45÷42.5 H
2	40.55÷41.5 H	42.45÷42.5 V
3	41.5÷42.45 V	40.5÷40.55 H
4	41.5÷42.45 H	40.5÷40.55 V

Fig. 2. Channel plan for digital MVDS.

Typical transmitters in lower frequency bands uses IF-modulation, followed by a combiner, a solid state amplifier and transmit antenna. With the today's state of the art amplifiers, a maximum output power of 3 to 5 W is achievable at 40 GHz. However, typical values are 0.5 to 1 W (national limitations), providing an output power per channel of 10 to 20 mW for 24 RF-channels (low-power MVDS), taking into account a output back off of 5 to 6 dB. To increase the output power for achieving larger service distances, each RF-channel can be build up separately without a combiner (high-power MVDS). Figure 3 shows

a proposal from Philips broadband systems. After the multiplexer, each RF-unit consists of a QPSK-modulator, upconverter, amplifier and sector-horn antenna with a gain of approximately 15 dBi. A transmitter unit including 8+1 redundant of such RF-units with one local oscillator is shown in Fig. 3, too. Hence, 4 of such transmitter units are necessary for each MVDS cell.

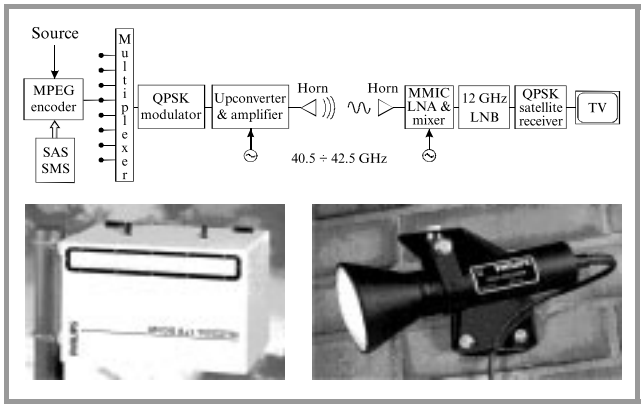

Fig. 3. High-power MVDS (each RF-channel is build up separately) from Philips broadband systems.

Close to the base station, a simple horn antenna can also be sufficient at the subscriber site, whereas pencil-beam antennas with very high gain are needed with increasing distance from the base station. This can be achieved by using paraboloidal or lens-horn antennas (Fig. 3), having a gain of around 30 to 36 dBi and 3-dB beamwidths of 5° to 2.5° for diameters of 10 to 20 cm.
Especially, the compact lens-horn antenna can easily be mounted on walls, is more aesthetic and causes much less mechanical problems due to wind forces than typical DBS antennas in the Ku-band. The receiving antenna is followed by a MMIC low noise amplifier and mixer, having a total noise figure of less than 6 dB. The mixer converts the received 40 GHz signal down to the 12 GHz region, where use can be made of standard DBS components (12-GHz LNB, a digital receiver and the TV).

3. LOS-propagation and service distances

The basic radio propagation characteristics and service area coverage of MVDS or LMDS systems is usually being limited to clear line of sight between the base station antenna and the customer antenna. Without atmospheric losses, the system gain is

$$G_s = P_{Tx} - L_{FTx} + G_T - L_R + G_R - L_{FRx} - N \quad [\text{dB}], \quad (1)$$

where

$$N = 10 \cdot \lg \left[k \cdot B_{RF} \cdot \left\langle \frac{T_A}{L_{FRx}} + T_F \left(1 - \frac{1}{L_{FRx}} \right) + \right.\right.$$
$$\left.\left. + (F-1) \cdot T_0 \right\rangle \right] \approx 10 \cdot \lg \left[k \cdot B_{RF} \cdot T_0 \right] + F \quad [\text{dB}] \quad (2)$$

is the thermal noise power, P_{Tx} the transmitter power, G_T and G_R the transmit and receive antenna gain, L_{FTx} and L_{FRx} the feeder losses, L_R the losses due to imperfect alignment, k the Boltzmann constant, B_{RF} the RF-bandwidth, F the noise figure of the receiver, T_A, T_F and $T_0 = 290$ K the antenna, feeder and the ambient temperature. The signal- or carrier-to-noise ratio C/N in the link budget is calculated by summing the system gain and the total path loss, including free-space attenuation $L_{fs} = 20 \cdot \lg \left[4\pi \cdot L/\lambda \right]$ with L for the distance and λ for the wavelength, clear sky attenuation A_{cs}, attenuation due to fog A_{fog} and rain attenuation $A_{h,v}(p)$:

$$C/N_{h,v}(p) = G_s - L_{fs} - A_{cs} - A_{fog} - A_{h,v}(p) \quad [\text{dB}]. \quad (3)$$

According to ITU-R Rep. 719-3 and 721-3, the specific attenuation during clear sky or due to fog are usually less than 0.25 dB/km or in between 0.05 to 1 dB/km for an average up to a high fog density at 42 GHz. The predominant factor affecting performance of LOS systems above 10 GHz is signal fading caused by heavy rain. Calculation starts from a knowledge of rain intensity statistics, e.g. those of ITU-R Rec. 837-1 for an average year, taking into account the climate zones $(CZ)E, H$ and K for variations across Germany, and an appropriate rain attenuation and cross-polarization model (Table 2) [5, 6].

Table 2
Rain intensity and specific attenuation (f = 42 GHz, horizontal polarization) for some percentages of time p of an average year and three climate zones E, H and K (ITU-R Rec. 837-1)

p [%]	Total time of a year	Point-rain rate R(p) [mm/h]			Specific attenuat. $A_h(p)$ [dB/km]		
		E	H	K	E	H	K
1	3.65 days	0.6	2	1.5	0.24	0.73	0.56
0.5	1.83 days	1.6	3.1	2.9	0.56	1.1	1.03
0.3	1.1 days	2.4	4	4.2	0.86	1.4	1.5
0.1	8.8 hours	6	10	12	2.0	3.2	3.8
0.03	2.6 hours	12	18	23	3.8	5.5	7.0
0.01	52 min.	22	32	42	6.7	9.4	12.1
0.003	16 min.	41	55	70	11.9	15.6	19.5
0.001	5 min.	70	83	100	19.5	22.8	27.0

In order to determine rain attenuation $A_{h,v}(p)$ use was made of a spatial rain model

$$A_{h,v}(p) = a_{h,v} \cdot \left[R(p) \right]^{b_{h,v}} \cdot L \ [\text{dB}]$$

for $R \leq 10$ mm/h and

$$A_{h,v}(p) = a_{h,v} \cdot \left[R(p) \right]^{b_{h,v}} \underbrace{\frac{1 - e^{-\gamma \cdot b_{h,v} \cdot \ln(R/10) \cdot L \cos\varepsilon}}{\gamma \cdot b_{h,v} \cdot \ln(R/10) \cdot \cos\varepsilon}}_{L \cdot \text{reduction factor } r} \quad [\text{dB}]$$

for $R > 10$ mm/h,

where $R(p)$ is the point rainfall rate (integration time of 1 min), p the exceeding probability of an average year, L the path length, $a_{h,v}$; $b_{h,v}$ the regression coefficients, depending on polarization, temperature, frequency and the drop size distribution, h and v the symmetry axes of the raindrop, ε the elevation angle and $\gamma = 1/14$ a fitting parameter for the rain profile (spatial decrease). Since the Laws-Parsons drop-size distribution characterizes the median values of statistical measurements well, the corresponding regression coefficients recommended by ITU-R Rep. 721-3 were used to determine cumulative distributions of an average year at 42 GHz. Because of paper limitations, all figures below are restricted to calculations for *CZ H* and horizontal polarization (worst case). For others see [5].

In order to illustrate trends in service areas, typical system parameters were assumed in the link budget of a digital MVDS: required $C/N = 6.8$ dB, $P_{Tx} = 0.5$ W, $G_T = 15$ dBi for a 64°-sector horn, $G_R = 32$ dBi for a lens-horn antenna, $F = 6$ dB, $B_{RF} = 33$ MHz, $L_R = 0.5$ dB, $L_{FTx} = 1$ dB and $L_{FRx} = 0.5$ dB. Figure 4 illustrates the coverage area of a 64°-sector horn transmit antenna of an elliptical, nearly circular shape. It is placed on the periphery has an azimuth pattern shown in Fig. 4. The effect of rain is quite apparent. For low rain rates, which correspond to low system availability percentages $(1 - p)$ in %, the service area is large. Conversely, the higher rain rate, or percentage availability, the smaller service area. To ensure that the target performance is maintained, e.g., for 99.9% of the time, the maximum service distance is nearly 6 km, compared to 27 km without rain. Because of this difference, an adaptive power control strategy seems to be reasonable, to reduce interference and EMC problems. The maximum service distance or the system margin at a given distance can be depicted from Fig. 5, where C/N is plotted vs. the service distance. For an average required C/N of 7 dB, the maximum service distance is approximately 6 or 3 km for an availability of 99.9 or 99.99% of the time.

Figure 6 exhibits the maximum service distance versus transmitter power per RF channel for a required C/N of 6.8 dB. A low-power MVDS with 10 to 20 mW meets the 99.9% criterion at a maximum LOS range of 2.5 to 3 km and a high-power MVDS with 0.5 to 1 W at 5.5 to 6 km.

MVDS especially in industrialized countries will only be competitive to CATV and DBS, if it can provide service-on-demand (SoD), i.e. if it can become a low-cost integrated medium with high-speed access to subscribers for interactive multimedia applications. For these interactive services an upstream or return path is needed from subscribers to the base station. Hence, interactive LMDS includes 1) a unidirectional forward broadcast path (FBP) for video, audio and data distribution, 2) a bi-directional interaction system composed of a forward interaction path (FIP) and a return interaction path (RIP) [1, 4]. The required data rates for interactive services are very dependent on the kind of services being requested. For example, video on demand, tele-shopping, or remote learning needs high bit rates of 2 to 6 Mbit/s in the FIP, whereas 20 kbit/s are sufficient in the RIP. In contrast, a video conference or an exchange of multimedia data needs in both interaction paths several Mbit/s. There are different strategies to meet these different data rate requirements and future service requests of customers 1) RIP and/or FIP are implemented out of band, offering low data rates via an external medium and, 2) RIP and/or FIP are embedded in the 2-GHz MVDS spectrum (in-band), able to provide higher bite rates up to several Mbit/s. The first option causes problems in combining the

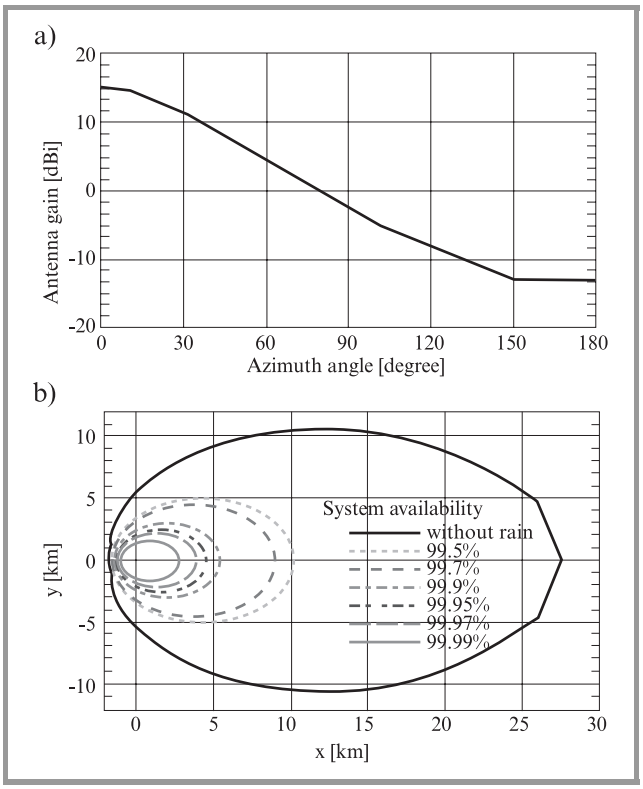

Fig. 4. (a) Azimuth pattern of a 64°-sector horn transmit antenna and (b) coverage area at 42 GHz for *CZ H* and horizontal polarization.

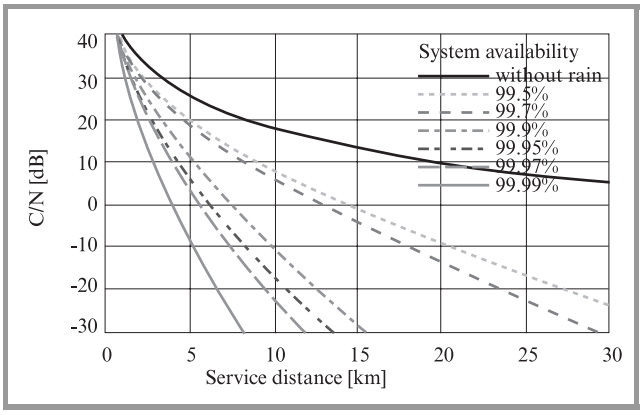

Fig. 5. C/N versus service distance for *CZ H* and horizontal polarization.

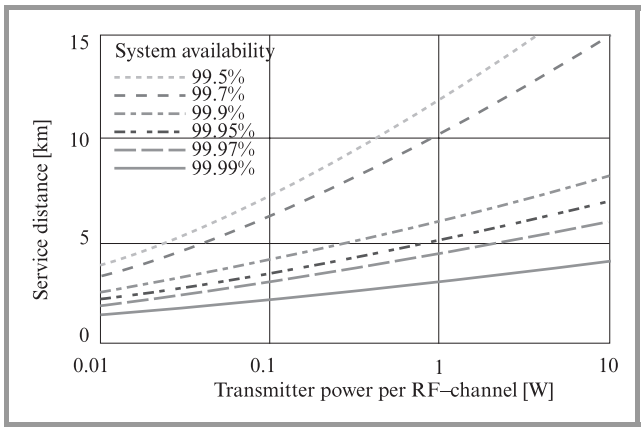

Fig. 6. Service distance versus the transmitter output power per RF channel for $C/N_{req} = 6.8$ dB, *CZ H* and horizontal polarization.

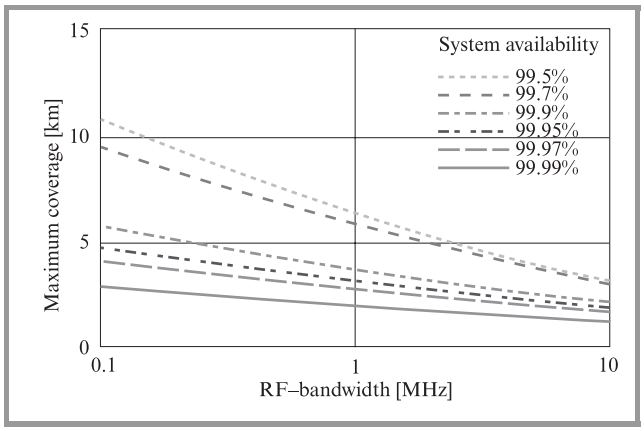

Fig. 7. Maximum coverage between customer station and base station versus RF-bandwidth of the RIP for an output power of 10 mW.

connections of FBP with external FIP and/or RIP, whereas transporting inter-active broadband services over a single wireless link seems to be more attractive from a customers point of view (single connection) and, it can be the only or at least a cost-effective solution for the competitors of the established operators in some areas. Therefore, solely the last option will be considered in this paper.

In order to keep the expenses of the customer station as low as possible, its complexity and transmitter output power should be low. Hence, robust modulation techniques such as QPSK or DQPSK without the need of a FEC is a good candidate. Figure 7 shows the maximum distance or coverage between customer stations and base station as a function of the RF-bandwidth of the RIP for an output power of 10 mW, where the 99.9% availability criterion meets the maximum LOS distance at 3.5 and 2.5 km for a bandwidth of 1 and 8 MHz. The distance can be increased up to 4 and 6 km for P_{Tx} of 100 mW [5].

4. The single-cell LMDS planing tool

The single-cell coverage prediction takes place in three steps as shown in Fig. 8. First, the number of visible households is calculated in order to select the best site for the base station, where usually only few sites are at one's disposal. Therefore, the visible parts of all buildings within the considered area have to be evaluated serving as input information for the household-estimation model, which will be presented below. All these calculations are based on 3D databases of both, buildings and vegetation. By the way, vegetation is here considered as blocking obstacles. This seems to be reasonable, because of large transmission losses of more than 30 dB above 26 GHz and the large time variations in the received power of up to 10 dB due to wind and seasons. Thus, a coverage through vegetation is not practicable at millimeterwaves.

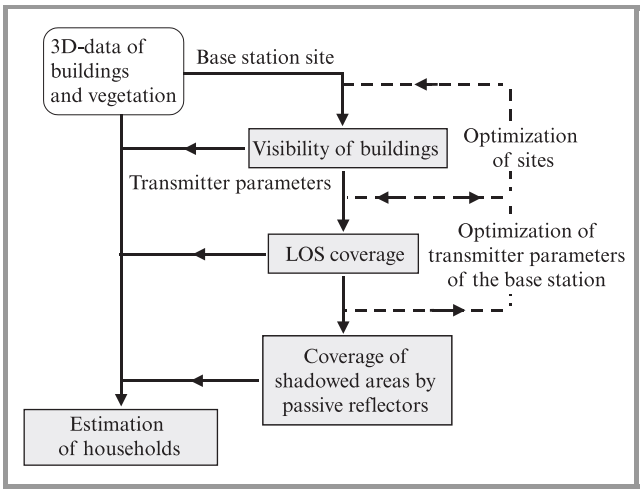

Fig. 8. Scheme of the single-cell LMDS planing tool.

Having selected the best site, the parameters of the base station's transmitter can be optimized in a second step, particularly the transmitter power and the orientation of the antenna in both, azimuth and elevation, by calculating the LOS area coverage under rainy conditions for certain rain climate zones. In a final step, specific reflectors can be used to increase the number of households by covering shadowed areas near the base station [9].

4.1. The household-estimation model

Firstly, it has to be defined what a potential customer might be. This is quite difficult, because this may vary with the provided application or service. Therefore, in our approach, a household is considered as an individual apartment or accommodation unit. This assumption is valid for most of the private buildings in urban or suburban areas, but will not be correct for public and business buildings representing just one customer, independent of the building size. To avoid any mistakes, additional residential information are needed.

The number of households within a building can be assessed either by the space-volume or the external surface of a house. Because a household is counted to be covered if at least a part of the corresponding surface of the building is covered, it seems to be reasonable to choose a surface-oriented algorithm rather than a space-volume-oriented method to estimate the number of households. Therefore, a building is represented by its surface consisting of walls and roof plains as shown in Fig. 9.

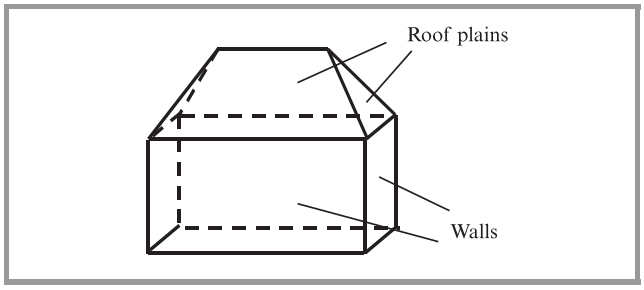

Fig. 9. Surface-oriented model of a building.

To estimate the number of covered households $N_{HH\,\mathrm{cov}}$, the covered parts of the building surface is needed. This input information has to be delivered by the planing tool. Hence, it has to be taken into account that the number of covered households depends not only on the size of the covered area but also strongly on the location of the covered parts. An example is shown in Fig. 10.

Therefore, the basic idea behind our household-estimation model is to choose the most probable location of a household in a building. Firstly, this is done by dividing a building into floors using an average floor height h_{floor}. In addition, the roof is treated as a floor, however with a weighting factor less than 1 or even neglected, depending on the declination of the roof. Furthermore, every wall is subdivided into several sections according to an average estimated length of a household l_{HH} as shown in Fig. 11. Of course several sections can belong to just one household.

Thus, by considering the floors separately, the calculation of the number of households N_{HH} and the number of covered households $N_{HH\,\mathrm{o}}$ becomes to

$$N_{HH} = \sum_{i}^{N_{\mathrm{floor}}} N_{HH,\mathrm{floor}}(i) \tag{4}$$

$$N_{HH\,\mathrm{cov}} = \sum_{i}^{N_{\mathrm{floor}}} N_{HH\,\mathrm{cov},\mathrm{floor}}(i)\ . \tag{5}$$

For the calculation of the number of covered households of a certain floor $N_{HH\,\mathrm{cov},\mathrm{floor}}$ it has to be taken into account, that one household can have several covered sections as shown in Fig. 12, where the household has to be considered only once.

A deterministic approach to avoid a multiple consideration of one household would be to define households and

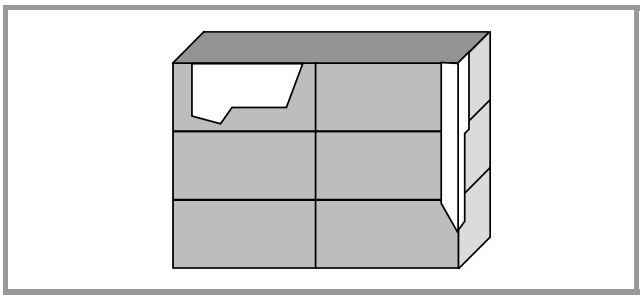

Fig. 10. Building with two visible parts of nearly the same size, but covering different numbers of households.

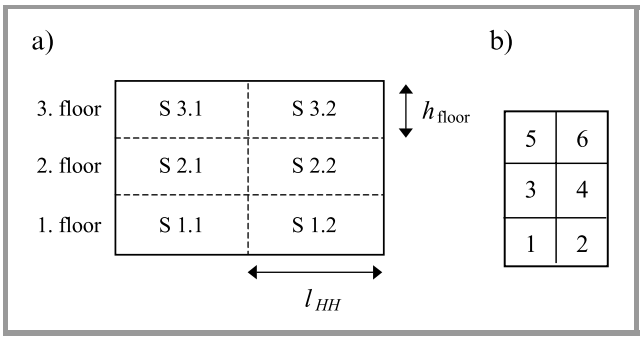

Fig. 11. Front sight of a single building wall (a) divided into floors and sections as well as the corresponding ground plane of the building with 6 households per floor (b).

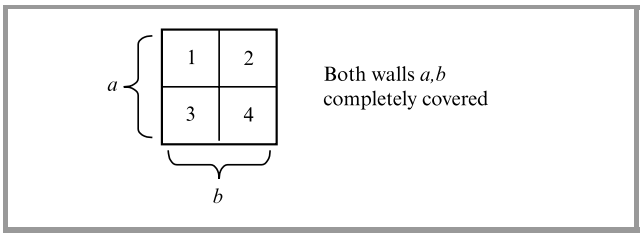

Fig. 12. One household (no. 3) with two covered sections.

assign the boundary sections to them. Then, also the number of households could easily be calculated. This method would be based on the assumption that the real households are essentially represented by sections, which generally is not valid. Therefore, in the following a more statistical algorithm is suggested for the estimation of $N_{HH,\mathrm{floor}}$ and $N_{HH\,\mathrm{o},\mathrm{floor}}$, respectively.

Obviously, there must be a correlation between the number of existent households per floor $N_{HH,\mathrm{floor}}$ and the number of sections of a floor $N_{S,\mathrm{floor}}$, depending on the shape of the building. For this correlation a good approximation is given by

$$N_{HH,\mathrm{floor}} = N_{S,\mathrm{floor}} - N_{\mathrm{convex}}\ , \tag{6}$$

where N_{convex} is the number of convex corners of a building.

Only the covered walls of the building are considered for the estimation of the covered households of a floor $N_{HH\,\mathrm{o},\mathrm{floor}}$.

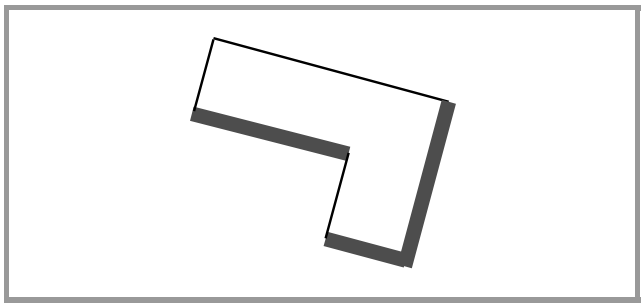

Fig. 13. Building with three covered walls (thick lines) and one covered convex corner $(N_{\text{convex,cov}} = 1)$.

A wall is counted to be covered, if only a part of it is covered. The percentage of covered sections of these walls are calculated and multiplied with the total number of all those households $N_{HH\,\text{walls,o}}$ with covered walls. Thus, the number of covered households of a floor is approximated by

$$N_{HH\,\text{cov,floor}} \approx \frac{N_{S\,\text{cov,floor}}}{N_{S\,\text{walls,cov}}} \cdot N_{HH\,\text{walls,cov}} \,. \tag{7}$$

Similar to the estimation of the existent households, the number of households $N_{HH\,\text{walls,cov}}$ with covered walls is computed from the number of sections $N_{S\,\text{walls,cov}}$ and the number of convex corners $N_{\text{convex,cov}}$ of the covered walls:

$$N_{HH\,\text{walls,cov}} = N_{S\,\text{walls,cov}} - N_{\text{convex,cov}} \,. \tag{8}$$

Here, a convex corner has to be formed by two adjacent covered walls as shown in Fig. 13.

The quality of our results of the presented model depends very much on the choice of the fitting parameters h_{floor} and l_{HH}, which have to be assessed on average from corresponding residential data. Therefore, a real validation of the suggested models requires a very large number of data, which has not been available yet. However, tests with buildings of the most common shapes show that the estimation of the number of existent households works quite well. In general, the results are getting more and more incorrect, the more complex the structure of a building is. However, because the estimation model for the number of covered households of a building and the model for the number of existent households of a building are quite similar, the quotient of both numbers, representing the percentage of coverage, will be quite accurate, even if the single estimations are not precise.

4.2. Design of passive reflectors to cover shadowed areas

In order to increase the number of covered households, particularly near the base station, the possibility to cover shadowed areas by using shaped metallic reflectors has been investigated for 42 GHz. In [11], use was already made of plane reflectors acting as passive repeaters. But covering additional households needs usually a much wider beamwidth, thus a reflector has to be convex. In fact, the

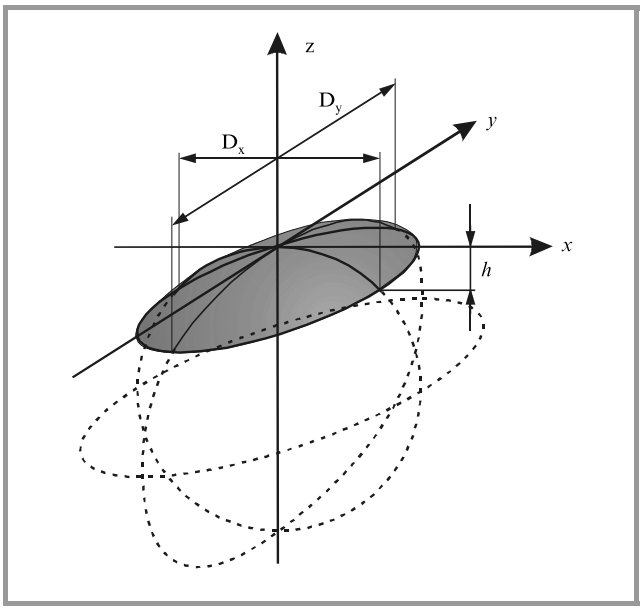

Fig. 14. Shape of the passive reflector.

radiation pattern of a passive reflector has to be adapted to a local situation, in order to cover as many customers as possible or aimed customers to be covered with LMDS, e.g. a shadowed street or building block. The required beamwidth in azimuth and elevation needs usually only a weak curvature of the reflector, i.e. only a slight deviation from a plane reflector. Hence, it is sufficient to consider merely a part of an ellipsoid with the diameters D_x and D_y or a part of a sphere $(D_x = D_y = D)$, both with the height h of the cap as shown in Fig. 14.

For both shapes, a pattern analysis using PO has been carried out in dependence of the height h, the diameters D_x and D_y as well as the angle of incidence of the incoming wave from the base station. In order to accelerate the computer speed to analyze the impact of passive reflectors applied in LMDS cells as well as for practical reasons, simple rules have been derived from the PO analysis for the design of metallic reflectors with a desired radiation pattern and gain [9].

The radiation patterns of a spherical reflector for different curvatures are shown in Fig. 15.

As you can see from Fig. 15, there are ripples in the main beam so that there is no real half power beamwidth (HPBW). Nevertheless, you can define a kind of average beamwidth Θ_{BW}, which seems to be proportional to the height h of the reflector, whereas the power density p decreases with h^{-2}. Including the influence of the diameters D_x and D_y you can find the approximations:

$$\Theta_{BW,\,\text{Az}} \approx 890^\circ \cdot \frac{h}{D_x} \;[^\circ] \tag{9}$$

$$\Theta_{BW,\,El} \approx 890^\circ \cdot \frac{h}{D_y} \;[^\circ] \tag{10}$$

for 3 mm $< h <$ 15 mm and 0.3 m $< D_x, D_y <$ 1 m.

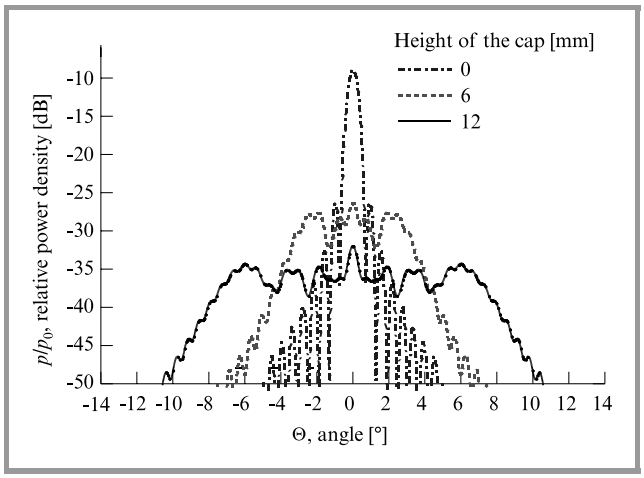

Fig. 15. Radiation pattern in a distance r = 150 m of a spherical reflector with infinite conductivity and a diameter of $D_x = D_y =$ 0.7 m for different heights h of the spherical cap and perpendicular incidence.

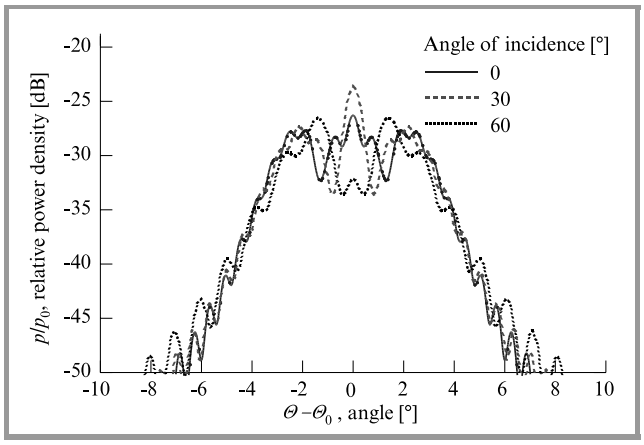

Fig. 16. Radiation pattern in a distance r = 150 m of a spherical reflector ($D_x = D_y = 0.7$ m, $h = 0.006$ m) with infinite conductivity and for different angles of incidence Θ_0.

Thus, the height h of a ellipsoidal reflector is determined by the maximum diameter corresponding to the smaller beamwidth. Another important result of the PO simulations is: varying the angle of incidence Θ_0 in a range of up to $\Theta_0 = 60°$ has nearly no impact on the average beamwidth Θ_{BW}, it causes only slightly different ripples as shown in Fig. 16.

The power density $p(r)$ at the observation point can easily be calculated by the following far-field expression

$$p(r) = P_R \cdot G \cdot \frac{1}{4\pi \cdot r^2}\,, \tag{11}$$

using an approximation for the "gain" of the reflector

$$G \approx \frac{4\pi}{\Theta_{BW,AZ} \cdot \Theta_{BW,EL}} \tag{12}$$

and the reflected power

$$P_R \approx p_0 \cdot \frac{D_x \cdot D_y \cdot \pi}{4}\,, \tag{13}$$

where p_0 denotes the power density from the source at the reflector surface and r the distance from the reflector.

This approximation has to be refined especially near the reflector. After introducing an additional empirical factor and defining a breakpoint r_1, we actually found the following approximations from the PO analysis:

$$\frac{p(r)}{p_0} = 1 \qquad \text{for } r < \frac{D_x \cdot D_y}{1.28\,\text{m}} \tag{14}$$

$$\frac{p(r)}{p_0} = \frac{1}{1.28\,\text{m}} \cdot \frac{D_x \cdot D_y}{r} \sim \frac{1}{r} \qquad \text{for } r < r_1 \tag{15}$$

$$\frac{p(r)}{p_0} = \frac{1.34}{\text{m}} \cdot \frac{1}{h} \cdot \left(\frac{D_x \cdot D_y}{r}\right)^2 \sim \frac{1}{r^2} \qquad \text{for } r > r_1 \tag{16}$$

with the breakpoint at

$$r_1 = 1.71 \cdot \frac{D_x \cdot D_y}{h}\,. \tag{17}$$

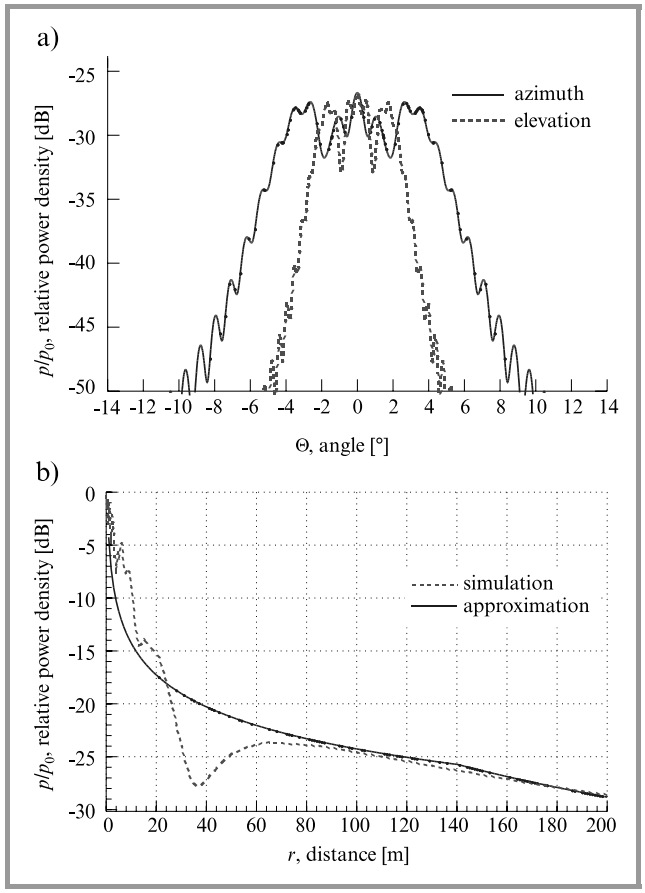

Fig. 17. (a) Radiation pattern in a distance r = 150 m and (b) relative power density as a function of the distance for an ellipsoidal reflector with D_x = 0.5 m and D_y = 1 m and height h = 0.006 m.

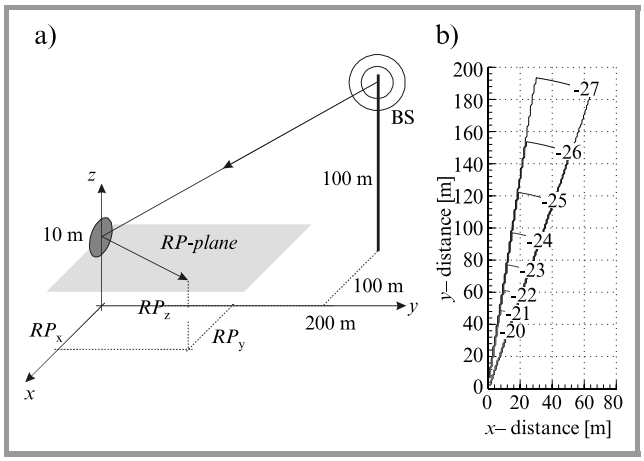

Fig. 18. Example of covering a shadowed street with a passive reflector: (a) layout of the arrangement: base station, metallic reflector ($D_x = 0.5$ m, $D_y = 1.0$ m, $h = 0.006$ m) and the receiving-point plane (RP), which is located 10 m above ground; (b) relative power density profile p/p_0 in dB in azimuth.

For a typical ellipsoidal reflector, Fig. 17 shows a good agreement of these approximations with the result of the PO simulations, the radiation pattern with PO (Fig. 17a) and the relative power density as function of the distance with PO (Fig. 17b). Obviously, there is a deep fading near the reflector. However, the fading only occurs very close to the boresight axis ($\Theta < 1°$) and can therefore usually be neglected.

In practice the size of the reflector is for aesthetic reasons limited to about 1 m. Because of the limited gain, the range of using passive reflectors is restricted to a distance of about 1 to 2 km around the base station. The range of the reflector's covering itself along the boresight is then up to about 200 m (Fig. 18), depending on the reflector's curvature or required beamwidth and the system margin [9, 10]. Thus, the usage of passive reflectors to cover shadowed areas is in principal possible and can be a cheap solution in certain areas, e.g. a shadowed street or building blocks.

5. Conclusions

A software tool for single-cell LMDS coverage prediction has been implemented based on 3D databases of buildings and vegetation. In order to provide the operator with information about the profitability of a cell, the desired number of potential customers has been approached by using simple household-estimation models. Apart from mere LOS considerations, also the coverage via shaped metallic reflectors has been investigated. Simple designing rules for these reflectors have been derived from detailed simulations at 42 GHz using PO. It shows that a passive reflector can be a cheap solution to cover shadowed areas for distances of about 1 to 2 km around the base station. As a next step, the multipath propagation effects caused by reflections and scattering on buildings and vegetation as well as co-channel interference have to be considered in the software planing tool. This has already been started in [12] and will be investigated in more detail in the near future using ray tracing techniques.

References

[1] H. Brüggemann, "DAVIC – Neue, weltweite Spezifikationen für digitale audiovisuelle und multimediale Dienste", *Telekom Praxis*, Nr. 2/96, 1996.

[2] "RACE DIMMP Workshop Papers", Metz, 1995.

[3] EN 300 748, "Digital Video Broadcasting (DVB); Multipoint Video Distribution Systems (MVDS) at 10 GHz and above", ETSI, 1997.

[4] EN 301 199, "Digital Video Broadcasting (DVB); Interaction Channel for Local Multipoint Distribution Systems (LMDS)", ETSI, 1998.

[5] R. Jakoby and M. Grigat, "MMDS zur Erweiterung von BK-Netzen", Research Report from TZ of Deutsche Telekom AG, 1996.

[6] R. Jakoby and F. Rücker, "Analysis of depolarisation events", PIERS, ESA Center, Noordwijk, CD-ROM, 1994.

[7] United Kingdom Radiocommunication Agency, "Performance Specification for Analogue/Digital Multipoint Video Distribution Systems (MVDS) Transmitters and Transmit Antennas Operating in the Frequency Band 40.5 – 42.5 GHz", United Kingdom RA, MPT 1550/1560, 1993/1995.

[8] U. Reimers, *Digitale Fernsehtechnik; Datenkompression und Übertragung für DVB*. Berlin-Heidelberg: Springer Verlag, 1995.

[9] R. Jakoby, G. Bauer, A. Hayn, and J. Freese, "Entwicklung von Ausbreitungsmodellen und Softwaremodulen zur Abschätzung der MWS-Versorgung unter Berücksichtigung von abgeschatteten Bereichen", Research Report for T-Nova, Deutsche Telekom, Germany, 1999.

[10] R. Jakoby and A. Hayn, in *Proc. 8th URSI Symp.*, Aveiro, Portugal, 1998.

[11] A. Vigants, "Space Diversity on a 6-GHz Path with Billboard Reflectors", ICC, 12B.1.-4, 1974.

[12] A. Hayn, R. Bose, and R. Jakoby, "Multipath propagation and LOS interference studies for LMDS architecture", in *Proc. ICAP 2001*, Manchester, UK, 2001.

Georg Bauer received his Dipl.-Ing. (M.Sc.) degree from the University of Stuttgart, Germany, in 1998. He is currently working as a Research Assistant pursuing a Ph.D. degree at the Institute of Microwave Engineering of the Technical University of Darmstadt, Germany. His research interests include wave propagation and broadband wireless access.

e-mail: g_bauer@hf.tu-darmstadt.de
Technische Universität Darmstadt
Institut für Hochfrequenztechnik
Fachgebiet Mikrowellentechnik
Merckstrasse 25
D-64283 Darmstadt, Germany

Jens Freese received the Dipl.-Ing. (M.Sc.) degree from the University of Siegen, Germany, in 1999. Since October 1999, he is working as a Research Assistant towards the Dr.-Ing. (Ph.D.) degree at the Institute of Microwave Engineering of the Technical University of Darmstadt, Germany. His research interests include adaptive antennas and microstrip antennas for millimeter wave applications.
e-mail: freese@hf.tu-darmstadt.de
Technische Universität Darmstadt
Hochfrequenztechnik
Fachgebiet Mikrowellentechnik
Merckstrasse 25
D-64283 Darmstadt, Germany

Rolf Jakoby – for biography, see this issue, p. 19.